X-ray Diffraction Topography of Germanium Wafers

Abstract: X-ray diffraction topography in transmission and reflection has been employed to analyze crystal faults and stresses in germanium wafers caused by deposition of oxide layers, epitaxy and planar diffusion. Localized diffusion of arsenic, gallium and phosphorus normally does not introduce stresses sufficiently high to generate dislocations in germanium (011) wafers. However, heat treatment of germanium wafers covered with a SiO₂ film causes high stresses which are often relieved by plastic deformation.

Introduction

In recent years X-ray diffraction topography has been increasingly employed to detect dislocations, stacking faults, elastic strains and misorientation in single crystals used in the manufacture of solid state devices. Such deviations from the ideal crystal structure may be caused either by the growth process or by a subsequent step of device fabrication, e.g., formation of oxide layers, diffusion of dopants, and epitaxial deposition, and they may influence device performance. Up to now, most topographic investigations were concerned with planar structures of silicon.^{1,2} With the growing interest in germanium for very fast devices it is obvious that this technique should also be used on germanium. Schwuttke3 has recently shown that X-ray topography can indeed be used for analysis of stresses in germanium wafers after planar diffusion. This paper deals with X-ray diffraction topography studies of basic device manufacturing steps in germanium and demonstrates its use for the analysis of defects and stresses introduced by thermal treatment, diffusion or epitaxial growth.

Transmission topography

• Contrast, wafer thickness and choice of X-radiation
The contrast between defect and perfect areas on a transmission topograph of a crystal wafer is determined by the intensity diffracted by a defect region and by a similar but perfect volume of the crystal. It depends on the structure factor F_{hkl} of the reflection used for the topograph, on the thickness D and the absorption coefficient μ of the wafer,

and on the wave length λ of the X-radiation. Figure 1 shows the thickness dependence of the intensity diffracted in symmetric transmission by a perfect crystal without absorption of the penetrating wave field⁴ and by a mosaic crystal with normal absorption. Optimal contrast is obtained for a thickness $D_0 = (\cos\theta)/\mu$ for which the mosaic crystal intensity has its maximum, θ being the Bragg angle. The intensity fluctuations of the perfect crystal give rise to the "Pendellösung" fringes on the topographs of wedge-shaped crystals.⁵ These fringes are often observed at the wafer edge beveled by the etch process (Figs. 2a, 3) and they demonstrate the perfection of the crystal. The ratio κ of the maximum of the mosaic crystal intensity to the mean perfect crystal intensity (which equals 1 in Fig. 1) can be used as a measure of the contrast. It is given by

$$\kappa = 2 Pr_0 \lambda F_{hkl}/(ve\mu), \qquad (1)$$

where P=1 or $\cos\theta$ for the two polarizations, $r_0=2.8\times 10^{-13}$ cm, e=2.718 and v is the volume of the unit cell. Table 1 shows the optimal thickness D_0 and the contrast κ for several wavelengths and the (220) reflection of silicon and germanium. With the most commonly used silver and molybdenum radiation, silicon gives a contrast about ten times higher and it allows the use of wafers about twenty times thicker than germanium.

Besides crystal thickness and wavelength, the contrast between perfect and faulty parts of the crystal also depends on the orientation of the diffraction vector \vec{g} in relation to the fault. For dislocations the contrast is minimal or maximal for $(\vec{g} \cdot \vec{b}) = 0$ or ± 1 respectively, where \vec{b} is the Burgers vector.

The author is at the Thomas J. Watson Research Center, Yorktown Heights, New York.

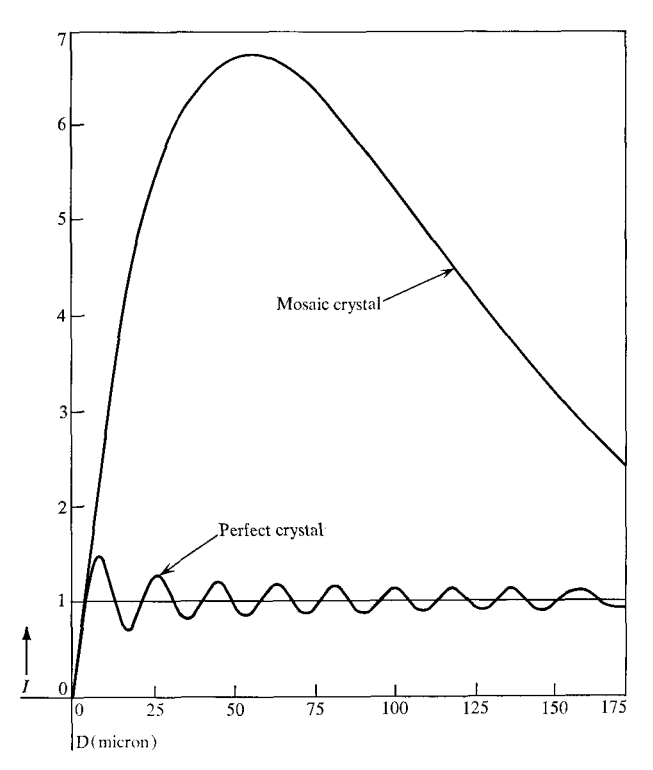


Figure 1 Intensity I diffracted in symmetric transmission by (022) planes of (011) Ge wafer of thickness D for a perfect crystal without wave field absorption (Ref. 4) and for a mosaic crystal with $Ag-K\alpha$ radiation.

• Geometry of image formation, resolution, and wafer size For the following discussion we assume the plane of the incident and diffracted beam to be horizontal. The horizontal extension of the image of an infinitesimal volume of the crystal, the horizontal resolution, is determined by the horizontal divergence of the diffracted beam $\Delta\theta$, which depends on the divergence of the incident beam and the rocking curve width, and by the sample-image plane distance r to be

$$S_h = r\Delta\theta. \tag{2}$$

The vertical resolution is determined by the vertical extension of the X-ray source F, the source-sample distance R and by r to be⁶

$$S_v = rF/R . (3)$$

With r being about 10 mm and for the Ag-K α -(220) reflection of germanium, the horizontal resolution is about 10 μ if the $\alpha_{1,2}$ doublet is not resolved and it can be considerably improved by decreasing the horizontal divergence of the incident beam. In order to achieve a vertical resolution of 10 μ , F/R in Eq. (3) has to be less than 0.001. Choosing a source-to-sample distance R of about 1.5 m the vertical focus extension F should not exceed 1.5 mm. This condition

Table 1 Optimal wafer thickness D_0 and contrast κ for (220)-topographs of germanium and silicon

| Radiation Wavelength (Å) | | W-Kα ₁ 0.2138 | Ag-K α_1 0.5594 | MO-Kα ₁ 0.7093 | Cu-Kα ₁ 1.5405 |
|-----------------------------|---------|-----------------------------|---------------------------|------------------------------|------------------------------|
| Ge: D_0 | (μ) | 750 | 55 | 29 | 17 |
| κ | | 36 | 6.8 | 4.4 | 8.4 |
| Si: D_0 | (μ) | _ | 1300 | 667 | 71 |
| κ | | | 66 | 44 | 10 |
| | | | | | |

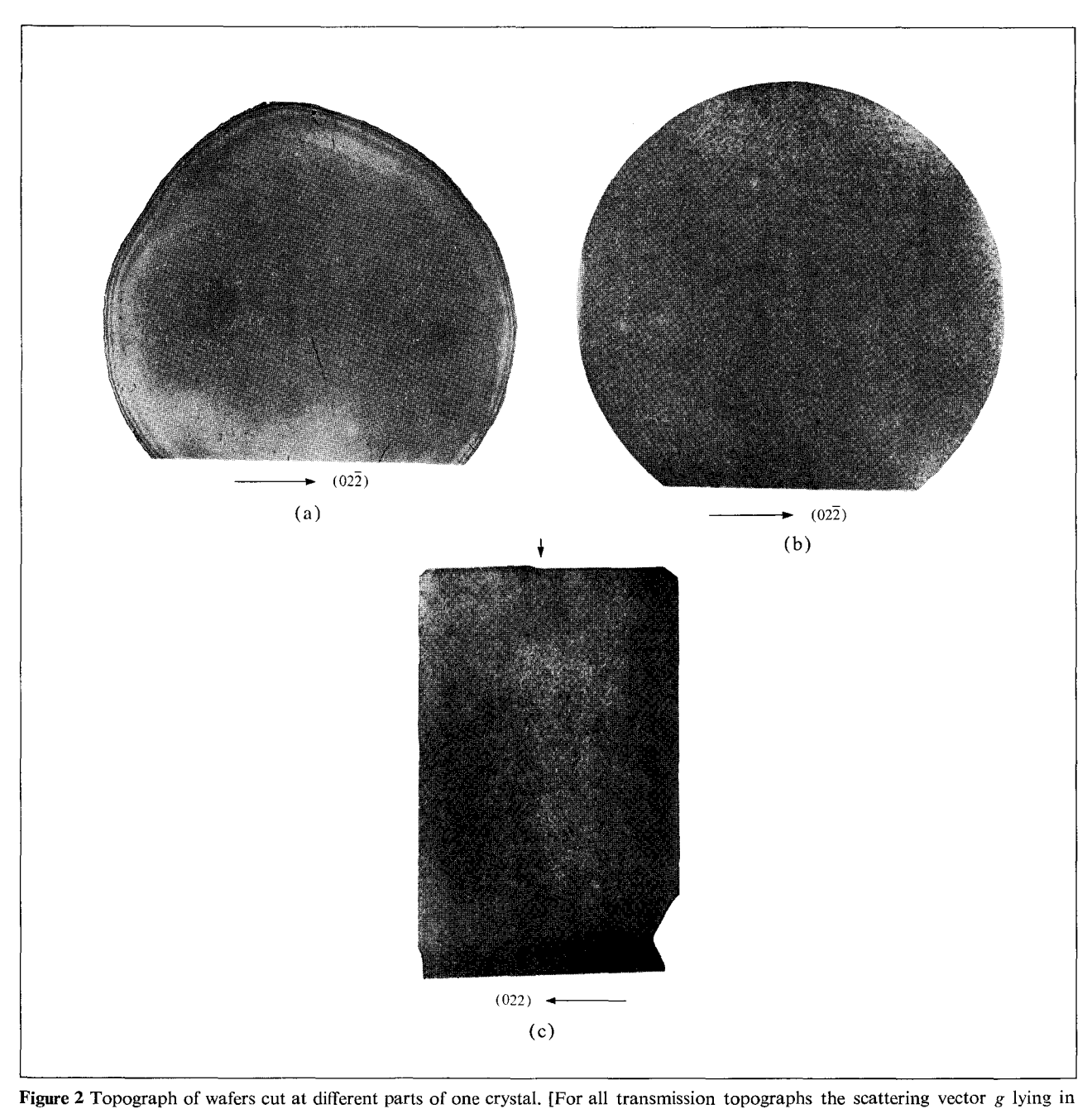
can be fulfilled by use of the spot focus of a normal diffraction tube with a 10×1 mm² focus, and if the take-off angle of 3° is chosen the horizontal divergence can be made sufficiently small without a big loss of intensity. Use of the line focus as suggested by Schwuttke to diffract over the full height of large wafers¹ reduces the vertical resolution by a factor of 10. Soller slits in the incident beam with the vertical divergence of 0.001 rad required to compensate for this loss of resolution would be extremely difficult to manufacture, and their use would result in a considerable loss of intensity. The spot focus is quite sufficient to get a topograph of a wafer, Z=25 mm high at a distance R=1.5 m from the focus, because the deviation from the Bragg condition in going from the center to the top or bottom of the wafer, as given by

$$d\theta = \tan \theta \cdot Z^2 / 8R^2 \approx 0.5 \cdot 10^{-5} \,\text{rad},\tag{4}$$

is far below the width of the rocking curve for the Ge (220) reflection with Ag-K α radiation.

• Experimental details

A GE silver tube operated at 50 kV and 16 mA was used as radiation source. The collimator slit was set to completely separate the $\alpha_{1,2}$ doublet of the Ge (220) reflection at $\theta = 8^{\circ}$. The other conditions were chosen according to the preceding considerations to assure a resolution of better than 10 μ . The topographs were recorded on Ilford G5 nuclear plates 50 \(\mu \) thick. A GE XRD5 Diffractometer was used with an x-y table mounted on it for scanning parallel to the horizontal wafer diameter and for adjusting the wafer to the diffractometer axis. Photographic plate, diffracted beam slits, and wafer were always kept parallel. Provisions were made to oscillate the sample during exposure using Schwuttke's Scanning Oscillator Technique¹ (SOT) to avoid the effects of macroscopic strains in the wafer. However, the oscillating range for germanium had to be restricted to about 0.3° in order to keep high the ratio of the topographic intensity diffracted only during part of the time and of the diffused background due mainly to fluorescence radiation. For the same reason a 12 μ thick palladium foil was inserted between sample and nuclear plate to preferentially absorb the fluorescence radiation. Occasionally a "ghost topograph" superimposed on the $0\bar{2}2$ topograph of



Magnification for all topographs is about $3 \times .4$ All topographs are positives; dark areas represent high diffracted intensity.]

a) $0.02\overline{2}$ transmission topograph is about $3 \times .4$ All topographs are positives; dark areas represent high diffracted intensity.]

a) $0.02\overline{2}$ transmission topograph of perfect (011) Ge wafer, center section of crystal, $\mu D \approx 1.5$ b) $0.02\overline{2}$ transmission of (011) Ge wafer with high dislocation density, rear section of crystal, $\mu D \approx 2$ c) $0.02\overline{2}$ transmission of (11 $\overline{1}$) Ge wafer cut parallel to growth direction (011), rear section of crystal, $\mu D \approx 3$.

a (011) wafer was observed, probably from the 111 reflection. A slight tilt of the crystal around the diffraction vector made the ghost disappear. The exposure time was determined by the scanning speed and only one scan was performed. Scanning speeds ranged between 3 and 10 mm/hr.

The germanium wafers were lapped on both sides with

garnet and polished on one side⁸ down to a thickness of 150 to 200 μ . The lap-damaged layer, which is thinner than 10 μ , was etched off with CP4.* To etch the wafer uniformly over the whole surface it was gently wiped with a "Q-tip"

^{* 120} cc HF, 200 cc HNO $_{\rm s}$, 120 cc CH $_{\rm s}$ COOH, 1 cc Br.

during etching. The final thicknesses of the wafers ranged between 100 and 300μ . The wafers were held in the sample holder between two thin plastic foils extended over a brass ring of 25-mm diameter. This method avoids gluing the sample and it does not introduce much strain if it is done carefully.

Reflection topography

• General considerations

Reflection topography was also used in certain cases. If appropriate asymmetric reflections are chosen the penetration depth is very small. This makes it useful for the investigation of thin surface layers or planar diffusion layers. For good resolution it is desirable to place the recording photographic plate approximately parallel to the wafer and approximately perpendicular to the diffracted beam. Therefore, larger Bragg angles are more generally used for reflection topography than for transmission topography.

Using Cu-K α_1 radiation the (333) or (115) reflection is very suitable on a (011) Ge wafer and the (115) likewise on a (111) Ge wafer. The angle of incidence α for these choices is about 10° and 6° respectively. This restricts the penetration depth perpendicular to the surface as given by

$$d = \sin \alpha / \mu \tag{5}$$

to 4 and 2.5 μ , respectively. Since in both cases the diffracted beam is almost perpendicular to the surface the photographic plate can be kept parallel to the wafer as in the transmission topography. However, the choice of a reflection of higher order, as in transmission, decreases the structure factor and contrast. The use of a higher Bragg angle increases $\Delta\theta$ and lowers the resolution.

Experimental details

The spot focus of a GE copper target tube with a take-off angle of 3° was used as radiation source of $0.5 \times 1~\text{mm}^2$ effective size. A 0.5-mm wide slit about 900 mm from the source restricted the horizontal divergence to 0.001. Diffracted beam slits were employed in order to decrease the background on the topograph. The scanning was performed parallel to the wafer and provisions for oscillating the sample and plate were made. The setup could also be used for transmission topographs with Cu-K α radiation without any major changes.

Defects arising during the growth process or heat treatment

Though the [011] growth direction—used for all the crystals of this study—does not favor the elimination of dislocations during the growth like the [111] or [100] growth directions, ¹⁰ dislocation-free Ge crystals can be grown in the [011] direction by the Czochralski process if dislocation-free seed

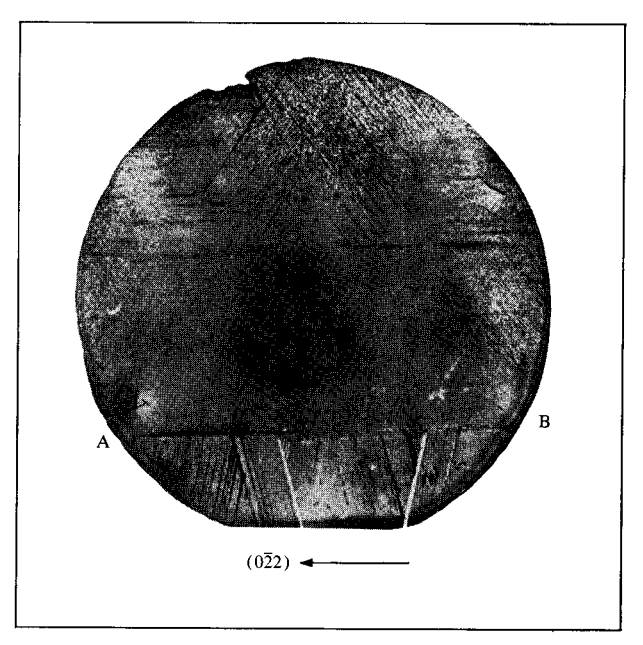


Figure 3 $0\bar{2}2$ transmission topograph of (011) Ge wafer cut from a crystal dislocation-free close to the seed, with dislocations and twinning generated during growth, $\mu D \approx 2$.

crystals are used. Figure 2a shows a 022 transmission topograph of a dislocation-free (011) wafer cut perpendicular to the growth direction from the center part of the crystal. However, during growth, dislocations, stacking faults or twinning may be introduced by thermal stresses or shocks. Figure 2b shows the 022 topograph of a (011) wafer cut from the rear end of the same crystal. To illustrate the generation of dislocations in this crystal a (111) wafer has been cut parallel to the growth direction. Its 022 topograph in Fig. 2c shows an abrupt increase of the dislocation density from a very low value of 300 cm⁻² at the right to a high value of 20,000 cm⁻² at the left. These numbers were measured independently by etch-pit count on the specimen surface. At the arrow the crystal had been remelted and growing had been restarted. The thermal stresses caused by this process introduced the dislocations.

Figure 3 shows the $0\bar{2}2$ topograph of a (011) wafer cut from another crystal which was dislocation-free at the seed end. Dislocations are arranged in (111) slip planes intersecting the (011) plane of the wafer in slip lines parallel to the $[0\bar{1}1]$, $[2\bar{1}1]$ and $[\bar{2}\bar{1}1]$ directions. Similar slip line patterns have been observed with etch methods by Penning¹¹ on cylindrical Ge crystals grown along [011] and quenched so as to produce a radial heat flow. They will be discussed in more detail in the next sample.

In addition to slip, twinning also occurred in this crystal during growth. The twin boundary along the line A-B is partly visible through the contrast of stacking faults extending from A to the center. Laue back-reflection photographs showed that the twinned part of the wafer below

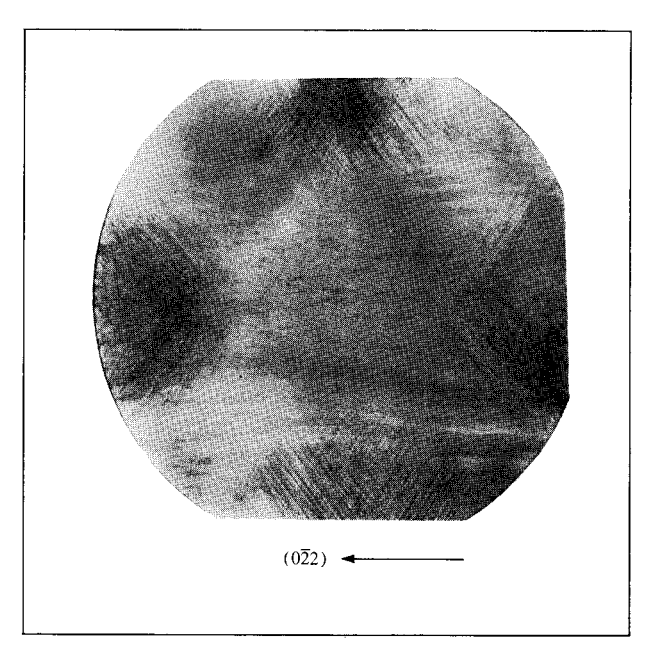


Figure 4 0 $\overline{2}$ 2 transmission topograph of (011) Ge wafer originally dislocation-free, after r-f heat treatment on cylindrical pedestal at 750°C, $\mu D = 2$.

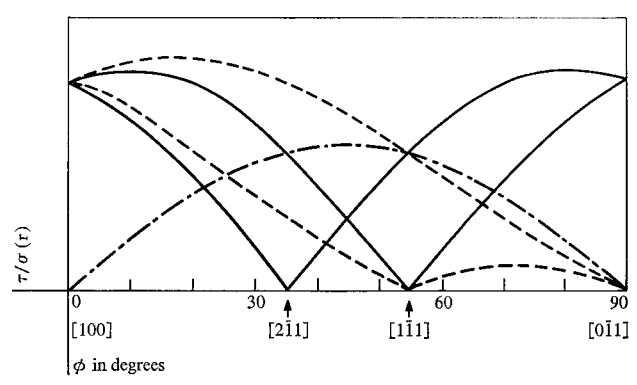


Figure 5 Resolved shear stress $\tau/\sigma(r)$ in different glide systems of circular (011) wafer with radial thermal stresses $\sigma(r)$ versus polar coordinate ϕ .

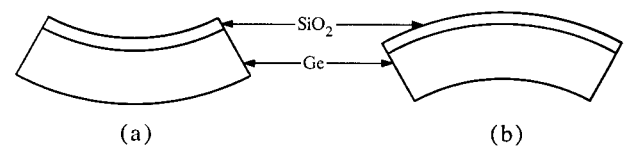


Figure 6 Germanium substrate with SiO_2 film, a) SiO_2 under tension, b) SiO_2 under compression.

A-B is parallel to the (411) plane. This plane can be brought into a position parallel to the (011) plane by a 180° rotation around the twin axis [111]. Both twins are in Bragg reflection since the diffraction vector is parallel to their common [0 $\bar{1}$ 1] direction. In the smaller twin, stacking faults are visible as dark bands. Secondary twins which are not in Bragg reflection any more appear white. The dislocations and twins were apparently caused by thermal stresses or shocks during growth. The center of the wafer is defect-free except for some polishing scratches.

Figure 4 shows the 022 topograph of an originally dislocation-free wafer after a heat treatment at 750°C on a cylindrical pedestal. Induction heating by a surrounding coaxial coil probably introduced large radial temperature gradients in pedestal and wafer. The distribution of slip lines is similar to that in Fig. 3. According to Penning¹¹ this pattern can be explained by the variation with ϕ of the resolved shear stress τ for the different slip systems of a wafer with radial thermal stresses $\sigma(r)$, r and ϕ being polar coordinates on the wafer (Fig. 5). If τ exceeds the temperature dependent critical shear stress on any slip system, slip is initiated in this system. Therefore, it can be seen from Fig. 5 that the slip systems giving rise to the oblique slip lines along [211] and [211] are not activated for 35° < $\phi < 55^{\circ}$. The more equally distributed horizontal slip lines along [011] are probably caused by radial heat flow as well as by heat flow normal to the wafer plane.11

Stresses in Ge wafers coated with SiO₂

An important step in the manufacture of planar devices is the pyrolytic deposition of SiO₂ on Ge wafers. ^{12,13} Due to the difference in thermal expansion of Ge and SiO2 elastic stresses are present in such wafers after cooling. The SiO₂ film may also be subjected to intrinsic stresses due to structural imperfection introduced by the process of formation. These stresses depend on the temperature of deposition and on subsequent heat treatment. If the residual stresses are large enough they can be recognized by a visible bending of the wafer. Figure 6 shows the two possibilities of tension (a) or compression (b) in the SiO₂. If a window is opened into the SiO2 for diffusion, then the stress is relieved inside the window and a large stress gradient is introduced normal to the window edges. If this stress gradient \vec{s} has a component parallel to the diffraction vector \vec{g} the image of the window edge on the topograph is either darker or brighter than the other parts of the wafer depending on whether $(\vec{s} \cdot \vec{g})$ is negative or positive.^{2,3,14} Figure 7 shows the 022 topograph of a wafer with windows $4 \times 4 \text{ mm}^2$ cut into the SiO₂ film pyrolytically deposited at 715°C. From the darkbright contrast sequence at opposite window edges along the diffraction vector, it can be concluded that the SiO₂ film is under compression (Fig. 6b). A "low temperature" SiO₂ film, deposited > 450°C in oxygen, 13 becomes under compression at room temperature; for deposition < 430°C, it becomes under tension. After densification at 750°C all

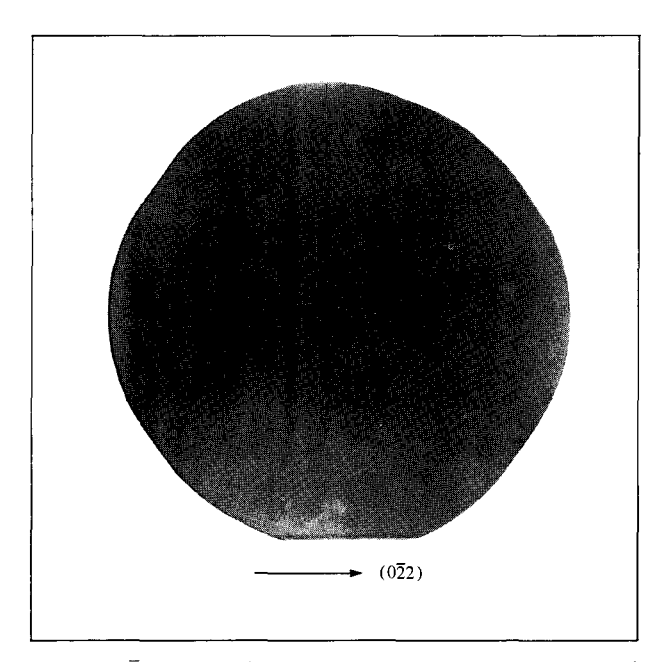


Figure 7 0 $\overline{2}$ 2 transmission topograph of (011)Ge wafer, coated with SiO₂ and with windows opened in the oxide, $\mu D \approx 2.5$.

low-temperature oxides are under compression. The stresses between the SiO₂ film and the Ge substrate are anisotropic, the direction of largest stress is the [100] direction. Upon removal of the SiO₂ film the stresses are completely relieved and the contrast at the window edges disappears. The fact that SiO₂ films deposited on germanium at temperatures above 450°C are under compression indicates that the thermal expansion coefficient of germanium is larger than that of the SiO₂ film, i.e., $\alpha_{\rm Ge} > \alpha_{\rm SiO_2}$. This is reasonable since the SiO₂ film is probably similar to vitreous silica, which has a very low thermal expansion coefficient. Unless they are partially relieved by plastic deformation the thermal expansion stresses become higher with higher deposition temperatures. This can be seen qualitatively, since the window edge contrast is very weak if the film is deposited at about 450°C and gradually increases with rising deposition temperature. However, at deposition temperatures below 430°C the intrinsic stresses override the thermal expansion stresses and, since they are opposite to the latter, they cause the film to be in tension.

On Ge wafers coated with high-temperature or densified low-temperature SiO_2 , dark and bright lines are often observed parallel to the traces of the (111) and ($\bar{1}11$) planes in the (011) plane of the wafer. These lines are not visible if the diffraction vector is chosen parallel to them (Fig. 8a) and they are clearly visible if the diffraction vector is perpendicular to them (Fig. 8b). Their dark-bright contrast

relation is reversed upon reversal of the diffraction vector, and they do not disappear upon removal of the oxide, as can be seen clearly in Fig. 8b, where the oxide is removed in the upper right quarter of the wafer. This rules out stresses in the interface as the cause of these lines. Since their contrast completely disappears on the $0\bar{2}2$ topograph (Fig. 8a) their fault vector must be perpendicular to the $[0\bar{1}1]$ direction. The good contrast in the 400 topograph (Fig. 8b) suggests the $\langle 111 \rangle$ or $\langle 211 \rangle$ directions perpendicular to the $[0\bar{1}1]$ for the fault vector whereas the [011] cannot be ruled out. These facts can be explained by stacking faults in the (111) and $(\bar{1}11)$ planes with fault vectors 1/3[111] and $1/3[\bar{1}11]$. Since the wafers are very thin, pronounced fringe patterns (as observed in silicon 15) would not be seen here.

Actually, Figs. 8a and b are topographs of a wafer taken after arsenic had been diffused into the open windows. However, these stacking faults are typical of those found in SiO₂ coated germanium wafers after heat treatment. They do not extend over the window area where the oxide had been removed. Also they have been observed on other wafers immediately after the pyrolytic deposition or the densification. They are generated during the plastic deformation caused by the difference in thermal expansion of germanium and SiO₂.

Diffused structures

All diffusion treatments were carried out through windows in the SiO₂ films described in the preceding paragraph. Arsenic was diffused into (011) wafers of N and P germanium in a two-zone furnace under a flow of forming gas. The As source was kept at 375°C for high surface concentration diffusion ($C_s = 5 \times 10^{19} \text{cm}^{-3}$, as measured by the method of corrosion potentials, 16) and the wafer was kept at 750°C. Stresses generated by the diffusion were opposite in sign to those generated by the high temperature SiO₂ film. This can clearly be seen in Fig. 8a, the 022 topograph of a wafer after arsenic diffusion. In the upper right quarter the oxide has been removed. At the right edge of the window there, the contrast is reversed from bright to dark, whereas all other window edges show the same contrast as do those in the topograph of Fig. 7. In the 400 topograph (Fig. 8b), where only the horizontal window edges are in contrast, the contrast has also been reversed at the horizontal edges of the upper right window where the oxide was removed, right of the vertical line ending at A. This indicates an expansion of the Ge lattice by the As diffusion. Since the tetrahedral radius of arsenic is slightly smaller¹⁷ than that of germanium ($r_{As} = 1.18 \text{ Å}, r_{Ge} = 1.22 \text{ Å}$) a contraction of the lattice would be expected for substitution of Ge by As atoms. Even if one assumes that part of the As atoms occupy interstitial sites and so expand the lattice, this effect should be overcome by the substitutional As atoms. Therefore, one has to assume that substitutional As atoms also expand the Ge lattice. Between the windows in the un-

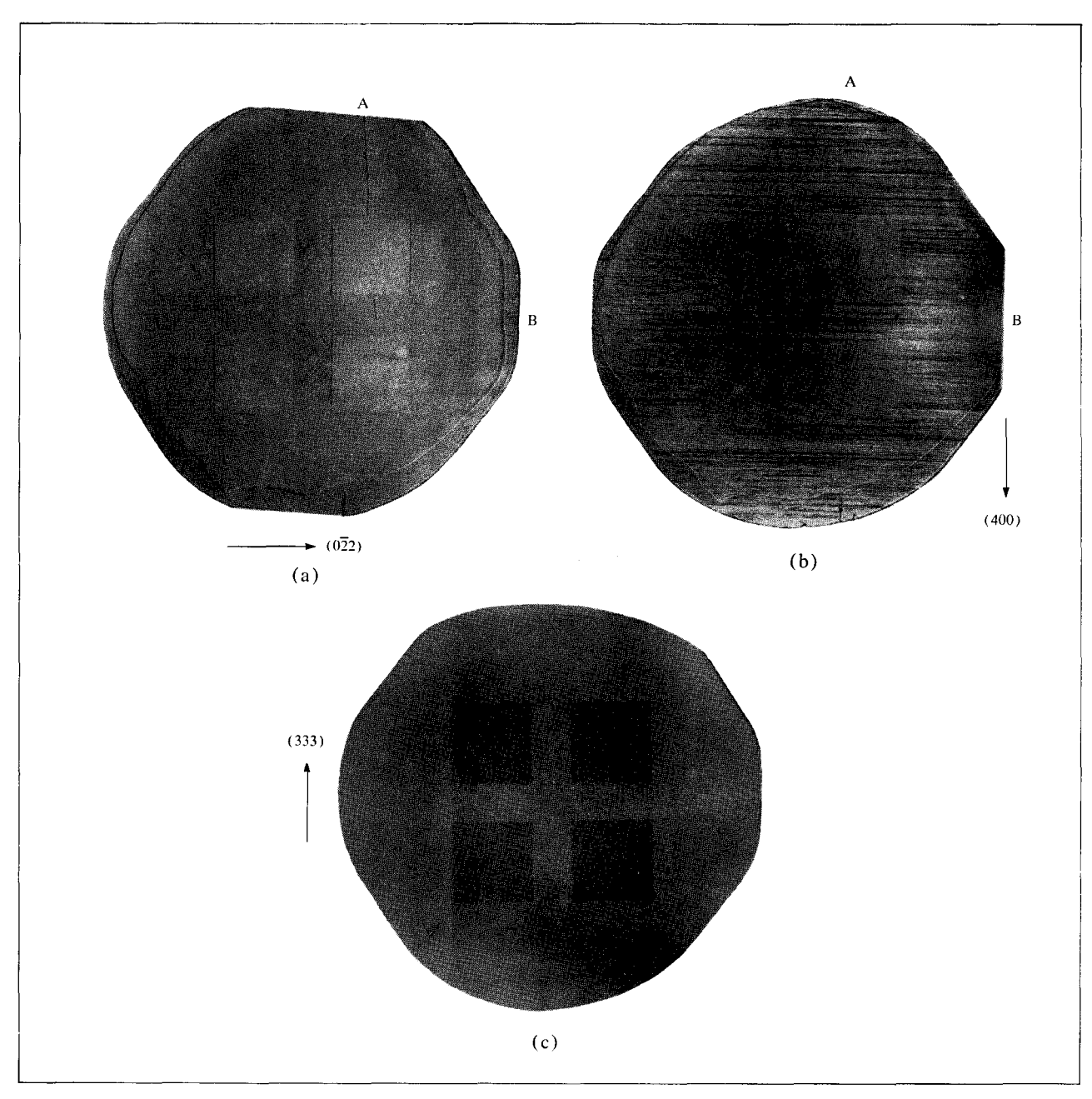


Figure 8 (011) Ge wafer coated with SiO₂, after arsenic diffusion through windows ($C_s = 5 \times 10^{19}$ cm⁻³; $x_j = 6.5 \mu$); $\mu D \approx 2$; the oxide is removed in upper right quarter in an area limited to the left by a vertical line ending at A and to the bottom by a horizontal line ending at B.

a) $0\overline{2}2$ transmission b) 400 transmission c) 333 reflection

diffused area a few slip lines are visible along [211] and $[2\bar{1}1]$, generated to relieve the stress from the expansion of the diffused areas.

Figure 8c shows the 333 reflection topograph of the Asdiffused wafer. The window area now diffracts with more intensity than the matrix. This contrast is further enhanced by choosing θ slightly smaller (0.04°) than $\theta_{\rm Bragg}$. It is decreased by choosing θ larger than $\theta_{\rm Bragg}$. This behavior also indicates a lattice expansion in the diffused area of the order of 0.1%. Measurements of the (022) rocking curve on a double crystal spectrometer in parallel position, as described by Cohen¹⁸ but with Ag-K α radiation, showed the lattice expansion to be $\Delta d/d = (0.86 \pm 0.08) \times 10^{-3}$ for $C_s = 5 \times 10^{19} \text{cm}^{-3}$ and $x_j = 6.5 \mu$. A contrast reversal as observed by Jungbluth¹⁹ in Cr-K α reflection topographs of phosphorus-doped emitter structures in Si

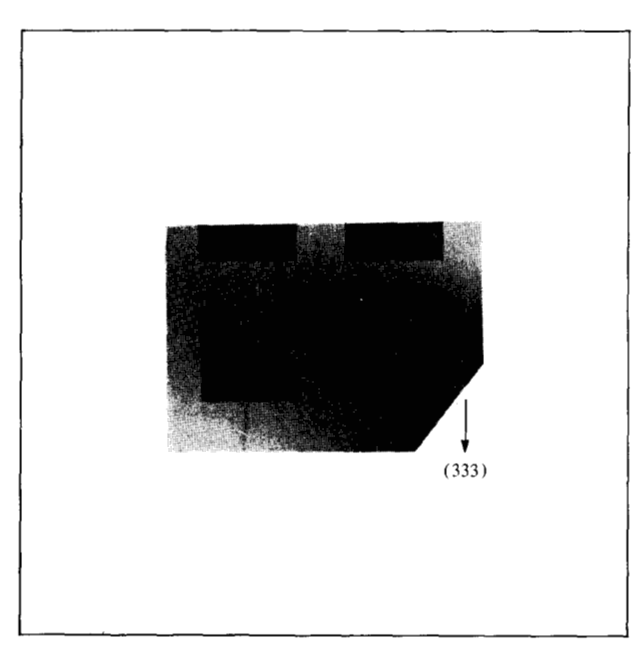


Figure 9 333 reflection topograph of (011) Ge wafer after arsenic diffusion ($C_s = 5 \times 10^{19}$; $x_j = 3\mu$). Diffusion has been barred where SiO₂ was not completely removed inside two windows.

could not be found when changing from $\theta < \theta_{\rm Bragg}$ to $\theta > \theta_{\rm Bragg}$. Therefore the contrast in the reflection topograph of As-doped structures in Ge is due to the higher intensity diffracted from the diffused areas. It cannot be explained in terms of lattice parameter differences only as it was suggested by Saccocio²⁰ for the contrast reversal observed by Jungbluth.¹⁹

Figure 9 shows the 333 reflection topograph of another As-diffused structure ($C_s = 5 \times 10^{19} \text{cm}^{-3}$, $x_j = 3 \mu$). The diffusion has been blocked where the SiO₂ had not been removed completely inside the window. The extinction contrast on the reflection topograph and the window edge contrast in the transmission topograph can still be observed for a junction depth $x_j = 0.65 \mu$ and a surface concentration $C_s = 3 \times 10^{19} \text{ cm}^{-3}$.

Gallium was diffused into N-type Ge at 800° C from a Ga-Ge source at 800° C for 16 hours to a surface concentration of 10^{20} cm⁻³ and a depth of $3.5~\mu$. A reduction of the window edge contrast but no reversal was observed after removal of the SiO₂. This indicates a very slight contraction of the diffused layer, though the tetrahedral radius of Ga is larger¹⁷ than that of Ge ($r_{\rm Ga} = 1.26~\text{Å}$). However, a sample diffused for 80 hours under the same temperature conditions showed an expansion of the diffused layer as evidenced by a contrast reversal at the window edges after removal of the SiO₂ film. This is in agreement with results obtained by Greiner²¹ who found a lattice parameter increase of 0.0004 Å per atomic percent of gallium dis-

solved in germanium. No intensity contrast has been observed between the diffused layer and the matrix, and no slip lines or dislocations were generated.

Phosphorus was diffused by heating the wafer at 750°C for 21 hours under an atmosphere of nitrogen with 1.4% PH₃. The surface concentration was $C_s = 5 \times 10^{19}$ cm⁻³ and the junction depth $x_j = 3.1 \mu$ as measured by the method of corrosion potentials. After removal of the SiO₂ film, the window edge contrast was reversed but it was very weak, indicating a very slight expansion of the lattice. Since the tetrahedral radius of phosphorus is smaller than that of germanium ($r_P = 1.10 \text{ Å}$, $r_{Ge} = 1.22 \text{ Å}$) we observe an effect similar to that seen in As-diffused wafers. No dislocations were generated by the phosphorus diffusion. Apparently the solubility of phosphorus in germanium is not high enough to cause dislocations to form by localized diffusion, as is observed²² in silicon for surface concentrations above 10^{20} P-atoms/cm³.

Arsenic was also diffused into (111) and (100) wafers with results similar to that observed on (011) wafers. However, Schwuttke and Howard³ have observed the generation of a few emitter edge dislocations on an arsenic-diffused (111) Ge wafer at the edge of the diffusion window. Possibly the (111) wafer is more apt to generate dislocation during diffusion than the (011) type.

Usually, because of the lower solubility of dopants in Ge, dislocations are less likely to be generated in Ge than in Si during diffusion. The dominant imperfections on such Ge wafers are stacking faults due to thermal expansion stresses.

Epitaxial layers on germanium

Epitaxial germanium layers doped with boron were grown on antimony doped N-type germanium at a temperature of about 800° by reduction of GeCl₄ (Ref. 23). The boron concentration, as measured by spreading resistance, corrected for multilayer structure, was about 5×10^{18} cm⁻³. The germanium wafers were coated with SiO₂ and windows were opened in the oxide; therefore epitaxy took place only at restricted areas. Figures 10a and b show the 022 transmission and the 333 reflection topograph of an epitaxially grown wafer after removal of the SiO₂ film. The epitaxial layers on the four square windows are perfectly crystalline; however, stresses can be observed by the contrast of the window edges in the transmission topograph. The contrast here is composite, as it is described by Howard and Schwuttke, 14 probably due to diffraction from the 5-µ thick epitaxial layer. The contrast is equal to that observed at windows cut into high-temperature oxide films. Therefore it can be concluded that the epitaxial layer, with a slightly lower lattice parameter, contracts the substrate material at the interface. The very bright seam along one edge of the windows, observed in the reflection topograph (Fig. 10b), is not a contrast effect due to stresses, but it is the shadow cast from the 5- μ high mesa by the X-ray beam, which is at a

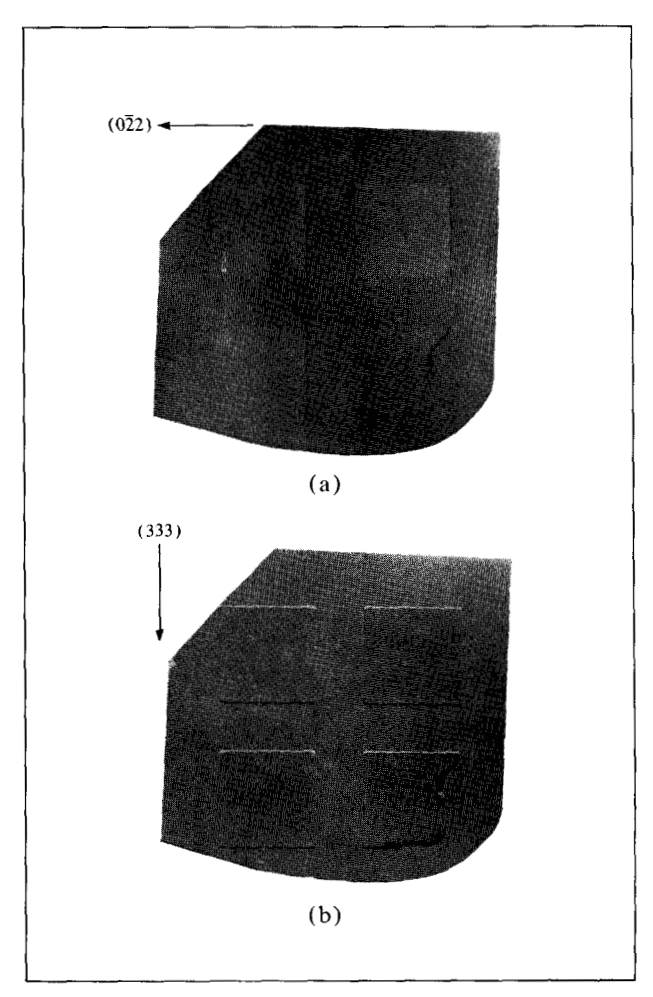


Figure 10 (011) Ge wafer, N-type 1 Ω -cm, $\mu D = 2.5$ with P^+ boron doped epitaxial layer 5 μ thick, $C \approx 5 \times 10^{18}$ cm⁻³.

a) 022 transmission b) 333 reflection

grazing angle of 10°. By accident not all oxide had been removed from one of the windows when they were opened and epitaxy had been avoided there, as can be clearly seen on both topographs.

Figures 11a and b show the (022) transmission and (333) reflection topograph of an indium doped *P*-type wafer with epitaxial boron-doped films grown through circular windows 0.125 mm wide and 0.750 mm spaced. Also here the epitaxial growth is perfect, stresses can be observed from the contrast and shadows are even more pronounced on the reflection topograph. On some areas too much oxide had been removed due to insufficient coverage with photo resist. No mismatch dislocations can be observed as described by Schwuttke¹ for boron-doped epitaxial silicon layers on silicon with much higher boron doping. Also here the solubility of boron in germanium is probably not high enough to cause sufficient mismatch, though differences in lattice parameters are observed by the resulting stresses.

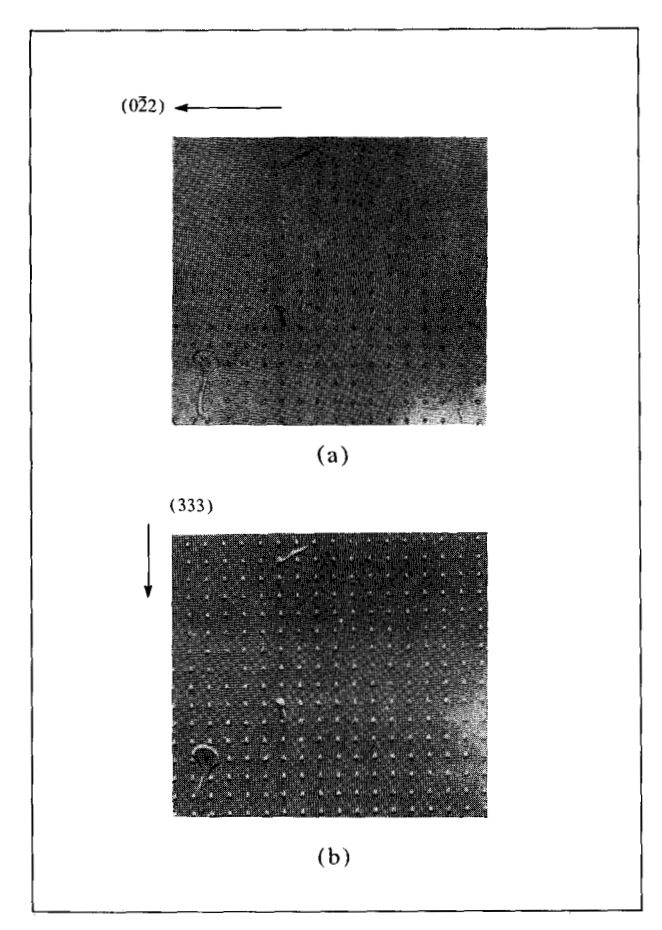


Figure 11 (011) Ge wafer *P*-type 0.3 Ω -cm with *P*⁺ boron doped epitaxial layer 5 μ thick, $C \approx 5 \times 10^{18}$ cm⁻³ deposited through circular holes of 0.125-mm diameter.

a) $0\overline{2}2$ transmission b) 333 reflection

Acknowledgments

It is a pleasure to thank R. Gereth for suggesting these investigations and for helpful discussions. I am also indebted to C. G. Wood for his valuable help in setting up the X-ray apparatus, and especially for implementing the Scanning Oscillator Technique. For preparing samples and measuring their properties I am grateful to E. Bassous, M. E. Cowher, M. J. Green, S. Krongelb, T. B. Light, R. L. Rohr, T. O. Sedgwick, V. J. Silvestri, and H. N. Yu.

References

- 1. G. H. Schwuttke, J. Appl. Phys. 36, 2712 (1965).
- 2. E. S. Meieran and I. A. Blech, J. Appl. Phys. 36, 3162 (1965).
- G. H. Schwuttke and J. K. Howard, J. Appl. Phys. 39, 1581 (1968).
- M. Laue, Rontgenstrahlinterferenzen; 3rd ed., Akademische Verlagsgesellschaft, Frankfurt am Main, 1960.
- 5. N. Kato and A. R. Lang, Acta Cryst. 12, 787 (1959).
- 6. J. B. Newkirk, Trans. AIME 215, 483 (1959).
- H. Cole, F. W. Chambers and C. G. Wood, Rev. Sci. Instr. 33, 435 (1962).

- 8. A. Reisman and R. L. Rohr, *J. Electrochem. Soc.* **111**, 1425 (1964)
- 9. J. K. Howard and R. H. Cox, Advances in X-ray Analysis 8, 35 (1965).
- 10. W. C. Dash, J. Appl. Phys. 30, 459 (1959).
- 11. P. Penning, Philips Res. Repts. 13, 79 (1958).
- 12. E. L. Jordan, J. Electrochem. Soc. 108, 478 (1961).
- S. Krongelb and T. O. Sedgwick, Electrochem. Soc., Electr. Div., Spring meeting May 1966, Cleveland, Ohio, Extended Abstracts 15, No. 54; S. Krongelb, to be published in Electrochemical Technology.
- 14. J. K. Howard and G. H. Schwuttke, Pittsburgh Diffraction Conf., November 9-11, 1966.
- K. Kohra and M. Yoshimatsu, J. Phys. Soc. Japan, 17, 1041 (1962).

- 16. R. Gereth, J. Electrochem. Soc. 113, 318C (1966).
- 17. L. Pauling, *The Nature of the Chemical Bond*, 3rd ed., Cornell Univ. Press, p. 244, 1960.
- 18. B. G. Cohen, Solid-State Electronics 10, 33 (1967).
- 19. E. O. Jungbluth, J. Appl. Phys. 38, 133 (1967).
- 20. E. J. Saccocio, J. Appl. Phys. 38, 3786 (1967).
- 21. E. S. Greiner, J. Metals 4, 1044 (1952).
- J. K. Howard and G. H. Schwuttke, Proc. 15th Ann. Cont. Applications of X-Ray Analysis, Eds., J. B. Newkirk and G. Mallet, August, 1966.
- 23. E. F. Cave and B. R. Czorny, RCA Review 24, 523 (1963).

Received June 3, 1968.